 doi:10.20944/preprints202007.0158.v1

Article

Catalytic activity of Srilankite nanoparticles in the esterification of oleic acid

Roberto Berrones-Hernández[1], Gerardo Trejo-Hernández[1], Yolanda C. Pérez-Luna[1], Yazmín Sánchez-Roque[1], Lizeth Rojas-Blanco[2], Ildefonso Zamudio-Torres[2], Sandra J. Figueroa-Ramírez[2], Germán Pérez-Hernández[2], Erik Ramírez-Morales[2]*

[1]Research laboratory, Universidad Politécnica de Chiapas, Carretera Tuxtla-Villaflores KM. 1+500, Las Brisas, C.P. 29150, Suchiapa, Chiapas, México.

[2] Universidad Juárez Autónoma de Tabasco. Avenida Universidad S/N, Zona de la Cultura, Col. Magisterial, Centro, C.P. 86040, Villahermosa, Tabasco, México.

[3] Facultad de Ingeniería, Universidad Autónoma del Carmen, Cd. del Carmen, Campeche, C. P. 24115, Mexico.

* Correspondence: eriking10@hotmail.com; Tel.: +527771528063

Abstract: . This work shows the results obtained in the synthesis of srilankite nanoparticles, (Zr, Ti)O_2, and TiO_2 anatase, both catalysts presented an admix of phases, anatase/rutile, and srilankite/rutile, respectively. Their performance in the production of biodiesel through the esterification of oleic acid was evaluated. The catalysts were obtained using the sol-gel process and sulfated via the impregnation method. The samples were characterized using X-ray diffraction (XRD), scan electron microscopy (SEM), energy-dispersive X-ray spectroscopy (EDS) and Fourier-Transform Infrared Spectroscopy (FTIR) to analyze the properties in its crystalline structure, morphology, and chemical composition. Its efficiency during the esterification reaction was measured based on the decrease in free fatty acids (FFA). FFA, oleic acid was added at different weight percentages (1%, 3%, and 5% w/w). The time of reaction was 6 hours at 55 °C and the catalyst with better performance was the sulfated Srilankite/rutile, reaching a maximum conversion of up to 90%.

Keywords: Esterification; Heterogeneous catalyst; Biodiesel; Srilankite; anatase; Nanoparticles.

1. Introduction

In the process of biodiesel production, the transesterification reaction is the most common process used. This kind of reaction is known as homogeneous catalysis, and it uses alkaline hydroxides. A deviation of this kind of reaction is to carry out the reaction under acid conditions [1]. The homogeneous catalysts (basic or acidic) has advantages like high activity (a reaction could be complete within one hour), it is not essential high temperatures and pressure (40 to 65 ° C and atmospheric pressure). At the industrial level, the homogeneous base catalysis is more commonly applied for biodiesel production because the base-catalyzed reaction is faster than the acid-catalyzed reaction [2].

However, homogeneous base catalysis causes soap formation; this leaves for the possible deactivation o the catalyst [3]. Other aspects are the difficulty of separating impurities, the removal of the catalyst after the reaction, the use of a large amount of water in the purification of biodiesel process and the generation of wastewater, all these aspects increase the production costs of biodiesel [4]. These disadvantages of homogeneous acid and base catalysis have promoted the research in heterogeneous

Preprints (www.preprints.org) | NOT PEER-REVIEWED | Posted: 8 July 2020 doi:10.20944/preprints202007.0158.v1

catalysts since they can activate the reaction process and allow easy separation from the reaction because they keep their solid phase [5].

During a process of heterogeneous catalysis, the catalyst and the reaction system are in different phases. At the finish of the reaction, the removal of the catalyst is simple, and its reuse is possible. Another aspect important about the heterogeneous catalysis is that throughout the process of obtaining biodiesel, glycerin of high purity is obtained, compared with homogeneous catalysis. Moreover, catalyst heterogeneous can be reusable; therefore, it makes the heterogeneous catalysts a better process than the homogeneous one and reducing costs [6].

Table 1. Advantages and disadvantages of the different kinds of catalysis and some examples of catalysts.

	Advantages	*Disadvantages*	*Example of catalyst*	*Reference*
Homogeneous base catalyst	High activity. Inexpensive and non-corrosive.	Formation of soap. No reusability.	NaOH, KOH, $NaOCH_3$	[7,8]
Homogeneous acid catalyst	Under mild conditions, the catalytic activity is enjoyable. Do not form soaps.	Long time reaction compared to homogeneous base catalysis. Corrosive. The separation of the products is complicated. Just once is usable.	H_2SO_4, H_3PO_4, CH_3SO_3H, AlCl3, $C_2HF_3O_2$	[9–11]
Heterogeneous base catalyst	Non-corrosive can be regenerated, reused, applied in continuous processes, and have easy separation of the obtained product.	Lower yields. The catalyst synthesis is expensive. The active sites have low efficiency.	Na_2CO_3, K_2CO_3, CaCO3, CaO, MgO, SrO, BaO	[12–16]
Heterogeneous acid catalyst	Easy separation. Is possible the use of the catalyst more once a time.	The catalyst synthesis is expensive. Deactivation of the catalyst is possible.	SO_4^{2-}/ZrO_2-TiO_2/La^{3+}, sulfated- Metal oxide	[17–20]

Between the heterogeneous base and acid catalysts, the last one presents advantages, because of its hydrophobic make the catalyst highly stable, this promotes high activity due to the presence of high acid site strength and minimal leaching of the active site [3,21]. This kind of catalyst also is used in esterification reactions. The production of biodiesel using heterogeneous acid catalysts improves the selectivity of the reaction, and avoid undesirable reactions such as saponification and possible uses in oils, with large amounts of free fatty acids [22]. Table 1 shows a summary of the advantages, disadvantages, and some examples of the different kinds of catalysts.

In order to develop heterogeneous acid catalysts for the production of biodiesel, many compounds have been investigated, acid-functionalized carbon [23], metal oxides/mixed metal oxides [24], and acid-functionalized metal oxides [25,26]. These catalytic reagents have shown good catalytic activity in the esterification of FFA [12,17]. Due to its excellent performance, there is a great interest in research related to the synthesis of these catalysts.

Preprints (www.preprints.org) | NOT PEER-REVIEWED | Posted: 8 July 2020 doi:10.20944/preprints202007.0158.v1

There are many methods for the preparation of the acid catalysts, self-assembly [23], coprecipitation [24], incipient wetness impregnation [27], hydrothermal [25], and sol-gel [28], this technique has many advantages, as low cost, control of the phase structure, better homogeneity, control in crystal size, monodispersity, and microstructure [26]. The most common method to make acid a catalyst is via impregnation whereby a metallic hydroxide, or oxide, interacts with a solution of H_2SO_4 or $(NH_4)_2SO_4$, followed by drying and calcination[12,29].

The importance of this work is in the absence of reports suggesting the Srilankite as an acid catalyst in the esterification reaction. The reaction catalytic to evaluate the performance of TiO_2 and Srilankite was conducted using esterification of oleic acid, employing both sulfated TiO_2 and sulfated Srilankite; first, the nanoparticles are obtained by the sol-gel method and after, they are sulfated via impregnation. The characterization of the compounds consisted of its crystal structure and morphology.

In this work, six main products were possible to obtain, which differ in the ratio of proportions of Ti and Zr precursors used, as well as in their immersion in a sulfuric acid solution, used to impregnate the TiO_2 and Srilankite catalysts with sulfur.

2. Materials and Methods

2.1 Reagents.

All the reagents used were by Sigma-Aldrich. Tetra-butoxide Titanium (Ti $(OC_4H_9)_4$) and zirconium propoxide (Zr $(OC_3H_7)_4$) as precursors for titanium and zirconium, respectively. Sulfuric acid at 95% was used to sulfate the catalysts. The acidity index was determined using reagents under the AOCS standard Ca 5a-40 and the NMX-F-101-1987.

2.2 Catalyst synthesis.

The synthesis of TiO_2 and (Zr, Ti)O_2 was carried out by the Sol-Gel Method, using Ti $(OC_4H_9)_4$ and Zr $(OC_3H_7)_4$. According to the literature, using this method is possible to obtain nanoparticles. The catalysts obtained were TiO_2, and the Srilankite, labeled as ZrO_2/TiO_2 1:3 and ZrO_2/TiO_2 1:4, prepared with a molar ratio of 1:3 and 1:4 of Zr and Ti, respectively. The gel obtained from the process was dried in an oven at 105 °C for 16 hours, the powder got was ground, then washed in ethanol. Subsequently, it was dried in an oven at 105 °C for 8 hours. Finally, it was calcined in a tubular oven at 550 °C for 3 hours under airflow of 5 min/h.

Table 2 shows the labels used for all the samples characterized and evaluated, also in the table, it is specified the precursor percentage used in the synthesis and if it was sulfated or not. These labels will be used from now on.

Table 2. List of the samples obtained indicating the rate of Zr and Ti precursor used during the synthesis. Also is indicated the sulfation of the catalyst.

Sample	*Rate (w/w %) (Zr $(OC_3H_7)_4$)*	*Rate (w/w %) (Ti $(OC_4H_9)_4$)*	*Sulfated*
TiO_2	0	1	No
TiO_2_1.5M	0	1	Yes
ZrO_2-TiO_2_1-3	1	3	No
ZrO_2-TiO_2_1-3_1.5M	1	3	Yes
ZrO_2-TiO_2_1-4	1	4	No
ZrO_2-TiO_2_1-4_1.5M	1	4	Yes

Preprints (www.preprints.org) | NOT PEER-REVIEWED | Posted: 8 July 2020 doi:10.20944/preprints202007.0158.v1

2.3 Sulfation catalyst.

The sulfation of the catalysts was carried out by simple impregnation with sulfuric acid (95% H_2SO_4). Three solutions of H_2SO_4 at different molar concentrations were used (0.5 M, 1 M, and 1.5 M). 0.25 L of the acid solution and 50 g of the catalyst were mixed and stirred for 3 hours. Afterward, by centrifugation, the solution was separated, and the sulfated catalyst was dried at 105 °C for 12 h in an oven to remove the water from the catalysts.

2.4 Characterization.

The characterization of the crystal structure for TiO_2 and Srilankite were realized by X-ray diffraction (XRD), in a RIGAKU SmartLab high-resolution diffractometer, using Bragg Brentano mode and CuKα radiation, at an acceleration voltage of 40 kV and a current of 44 mA. The measure scanned was carried out in a $\theta/2\theta$ range of 20°- 70°, at a scanning speed of 4° min-1. The morphology was observed in an SEM JEOL JSM-7100F equipment at 5 kV acceleration voltage under high vacuum conditions.

Energy dispersion spectrometry (EDS) and Fourier Transform Infrared Spectrometry (FTIR) techniques were used to determine the elemental composition and the chemical species, respectively. To carry out the EDS analysis, a detector coupled to the SEM (JEOL JSM-6010LA) for a semiquantitative analysis and distribution of elements on the surface of the samples, was used. For the IR analysis, a pellet using a mix of the sample with KBr (Sigma Aldrich grade FTIR) at a concentration of 10% w/w, was prepared. Then, analysis in a Shimadzu Mod. IRAFfinity-1 FT-IR spectrometer, in a range of 4500 cm^{-1} - 400 cm^{-1}, at a resolution of 2 cm^{-1} and 40 scans, were realized.

2.5 Reaction procedure.

The esterification reaction was carried out to evaluate the performance of the catalysts in a three-neck glass reactor in a temperature range from 50 °C to 55 °C, and the pressure at room conditions. The molar ratio of oleic acid and methanol of all reactions was 1:15. Different catalyst concentrations respect to oleic acid were used (1%, 3%, and 5% by weight). The variation of the acid number (AIm) and the variation of free fatty acids (FFA), from the oleic acid, was calculated with the methodology of the AOCS standard Ca 5a-40 and the NMX-F-101-1987. The conversion of oleic acid to methyl oleate (methyl ester), was obtained with the following equation:

$$Conversion(\%) = \left(\frac{A\,\mathrm{Im}}{Aoleic} \right) * 100$$

Where AIm and AIoleic indicate, the acid number of the sample measured during the reaction and the acid number of the oleic acid at t = 0, respectively, 20,21.

2.6 Statistical analysis.

The estimation of the percentage conversion was using a factorial design, considering three treatments T1: Composition of the catalyst (TiO_2, ZrO_2/TiO_2 1:4, ZrO_2/TiO_2 1:3); T2: concentration of sulfation solution (1.5 M) and T3: percentage of catalyst (1%, 3%, and 5%), each sample with three levels and three repetitions. The results obtained were analyzed by Analysis of Variance (ANOVA) and Least significant difference (LSD), using the Infostat software (version 2017.1.2).

3. Results

T*3.1 Catalyst characterization*

In Fig. 1, it is possible to observe the XRD diffractograms of the different samples. Fig 1a shows the XRD patterns for the samples TiO_2 and TiO_2_1.5M. In the plots, it is possible to identify the peaks at approximately 2θ = 25.3°, 37.8°, 48.8°, 53.9°, and 62.7° corresponding to the crystalline planes (1 0 1), (0 0 4),

Preprints (www.preprints.org) | NOT PEER-REVIEWED | Posted: 8 July 2020 doi:10.20944/preprints202007.0158.v1

(2 0 0), (1 0 5) and (2 0 4), respectively, for anatase phase. Additionally, the peaks for the rutile phase were observed in the same sample, founding them at approximately 27.44° and 69.0°, corresponding to the planes (1 1 0) and (3 0 1), respectively. It is possible to observe no considerable changes in the TiO_2 before and after to be immersed in a 1.5 M H_2SO_4 solution. Through these observations, it is evident that using the method of synthesis here reported; it is viable to obtain the admix of phases above mentioned and, the sulfation process does not affect the phase structure.

Figure 1b shows the diffractograms for the samples obtained using different rates of Zr and Ti precursors (1:4 and 1:3) and its corresponding sulfated samples. In the plots, it is possible to observe the characteristic XRD peaks for rutile phase, at around 2θ = 27.3°, 54.55°, 69°, and 69.6° corresponding to the crystalline planes (110), (211), (301) and (112), respectively. Moreover, the peaks for Srilankite phase were identified at 2θ = 24.6°, 30.6°, 32.57°, 35.82°, 37.11°, 38.5°, 40.68°, 42°, and 53.37°, with the crystalline plane (110), (111), (020), (002), (021), (200), (102), (121), (130), respectively.

The results above presented suggest that ZrO_2-TiO_2_1-3 and ZrO_2-TiO_2_1-4 and their corresponding sulfated sample (ZrO_2-TiO_2_1-3_1.5M and ZrO2-TiO2_1-4_1.5M), has an admix of phases (rutile and Srilankite). Another observation is the notorious decrease intensity of the peaks in the samples ZrO_2-TiO2_1-4 and its respective sulfated sample; in comparison with ZrO_2-TiO_2_1-3 and its respective sulfated sample, this suggests a decrease in the crystallite size because of the hydrolysis reaction leading to the formation of original nuclei or basic units. In particular, the effect of the concentration ratio [Men+]/[H+], leads to decrease in particle size [30]; another observation is that after the sulfation is the absence of the anatase phase, due to rebuilding of the Srilankite phase, according to a similar observation made by Li et al. [25].

Table 3. Crystallite size calculated from Scherrer equation.

Catalyst	The crystallite size (nm)
TiO_2	15.48
TiO_2_1.5M	14.37
ZrO_2-TiO_2_1-3	16.95
ZrO_2-TiO_2_1-3_1.5M	16.59
ZrO_2-TiO_2_1-4	17.44
ZrO_2-TiO_2_1-4_1.5M	17.09

The crystallite size was calculated using the Scherrer equation [31], taking a form factor of 0.90, an X-ray wavelength of 1.5406 Å, the width at the average height of the diffraction peak (FWHM) of the principal peak, (1 0 1) and (1 1 0), for Anatase and Srilankite phases, respectively. Table 3 shows the results obtained. The results in crystallite size are according to the above discussed.

Preprints (www.preprints.org) | NOT PEER-REVIEWED | Posted: 8 July 2020 doi:10.20944/preprints202007.0158.v1

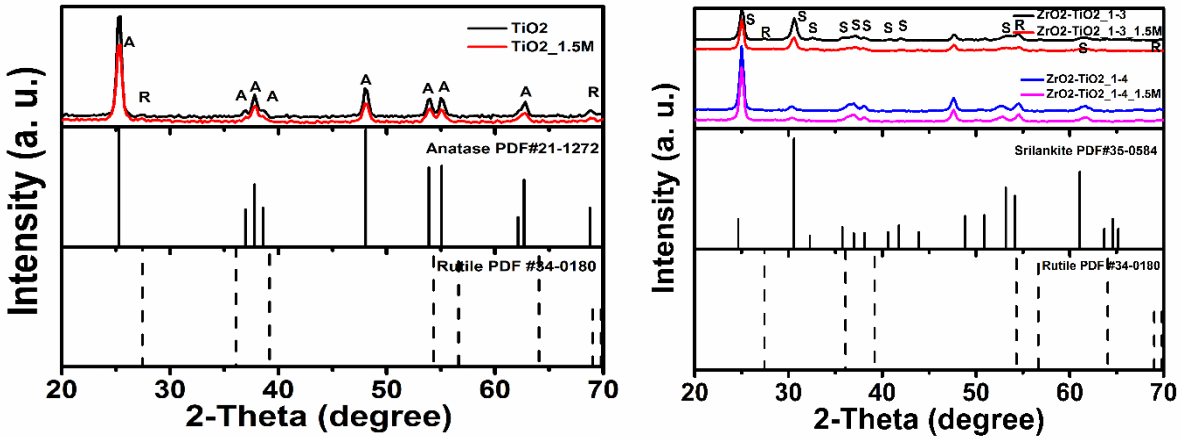

Figure 1. X-ray diffractograms for the samples obtained, according to Table 1. Anatase (A), Rutile (R), and Srilankite (S) phases and its patterns are identified and shown.

Figure 2 shows the FTIR spectra analysis. The spectra reveal the composition of materials and functional groups present in the samples. The objective of this study is to analyze the nanocatalysts TiO_2, TiO_2/Srilankite, and their sulfated samples to observe the significant presence of the sulfate ion.

In general, for all Figure 2, the spectroscopic bands observed between 3600-3000 cm^{-1} describe both the symmetric and asymmetric stretching vibrations of the hydroxyl group (OH). The wideband observed is related to the vibrational stretching mode of the hydroxyl groups, indicating the presence of moisture in the sample, and peak at 1630.81 cm^{-1} is associated with the O-H bending vibrations of the water molecules absorbed. Therefore, the peaks observed at around 3600-3000 cm^{-1} and 1640 - 1600 cm^{-1} correspond to water adsorbed on the surface and to hydroxyl groups [32].

Peaks in ranges of 2400 - 2300 cm^{-1} and 1300 - 950 cm^{-1} are associated with the stretching mode of the CO_2 molecule, and symmetrical vibration of stretching of the S-O bonds of the sulfate groups, respectively [25,33,34].

The bands at around 1070 - 1045 cm-1 correspond to the symmetric stretching of S=O bonds of the sulfate groups [34]. The broadband of the region of 1000 to 400 cm^{-1} corresponds to the Ti-O stretch and Ti-O-Ti stretch modes. The peaks at 573.85, 525.62, and 515.98 cm^{-1} correspond to the symmetrical Ti-O-Ti stretch, and the ranges of 800-400 cm^{-1} suggest the anatase phase of [35,36].

In general, IR spectra of compounds labeled ZrO_2-TiO_2 (1-3 and 1-4) present a difference to the TiO_2 spectrum, due to the incorporation of Zr precursor, with peaks in the range of 700 - 400 cm^{-1} [37], the peaks between the 745 - 490 cm^{-1} ranges are assigned to the asymmetric vibrational stretches Zr-O-Zr, this confirms the presence of the Srilankite phase.

In Figure 3, the results of the characterizations by SEM show images obtained at 50,000 X, observing an agglomeration of particles showing spherical morphology. Although SEM micrographs showed that the catalyst morphology was not affected by the sulfation process in the same material, it is possible to observe a slight increase in particle size as the amount of ZrO_2 in the material increased (approximately 9-13%). TiO_2 (Figure 3a-c) presents the smallest particle size compared to the sample ZrO_2-TiO_2_1-3 (Figure 3d-f) and ZrO_2-TiO_2 1:4 (Figure 3g-i). The increase in particle size may be related to a larger atomic radius size of zirconium relative to titanium (Zr = 206 Å, Ti = 176 Å). This result is consistent with those obtained from the calculation of particle size made with the Scherrer equation [38].

The composition of the material employing the EDS technique is shown in Figure 4. The graphs show the elemental composition of the sample in Figure 4a) (TiO_2), the presence of Zr and its increase gradually are visible, according to the methodology used which increases the rate of Zr in the samples ZrO_2-TiO_2_1-3 and ZrO_2/TiO_2_1-4, shown in Figures 4b) and 4c), respectively. In Table 3, the composition data derived from the EDS analysis, are shown. Quantitatively the Zr concentration in ZrO_2/TiO_2 1:3 is 26.31% weight, 4.06% more than sample ZrO_2/TiO_2_1-4.

Preprints (www.preprints.org) | NOT PEER-REVIEWED | Posted: 8 July 2020 doi:10.20944/preprints202007.0158.v1

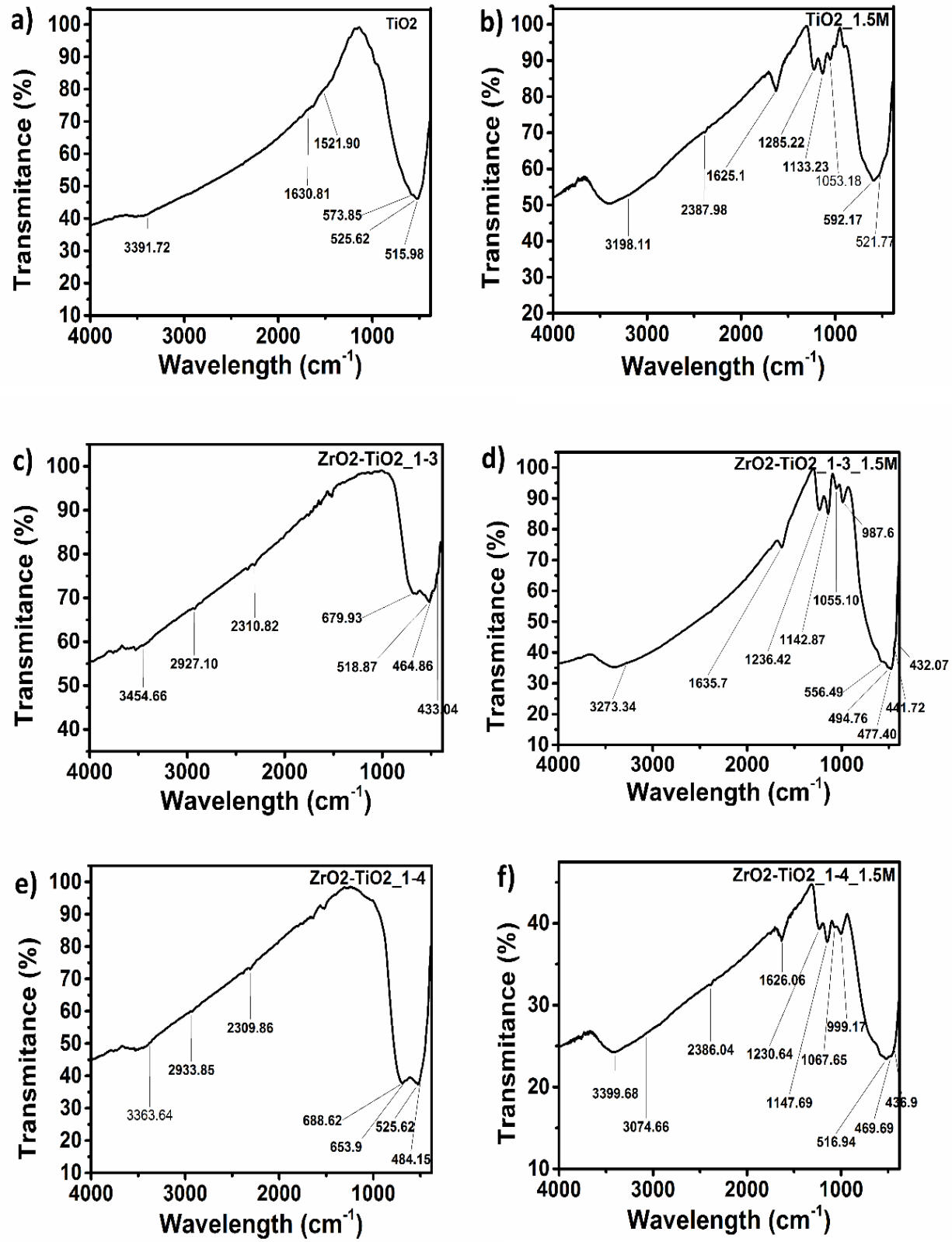

Figure 2 IR spectra for TiO_2 and Srilankite samples. a)TiO_2, b)TiO_2_1.5M, c)ZrO_2-TiO_2_1-3, d) ZrO_2-TiO_2_1-3_1.5M, e)ZrO_2-TiO_2_1-4, f)ZrO_2-TiO_2_1-4_1.5M.

Preprints (www.preprints.org) | NOT PEER-REVIEWED | Posted: 8 July 2020 doi:10.20944/preprints202007.0158.v1

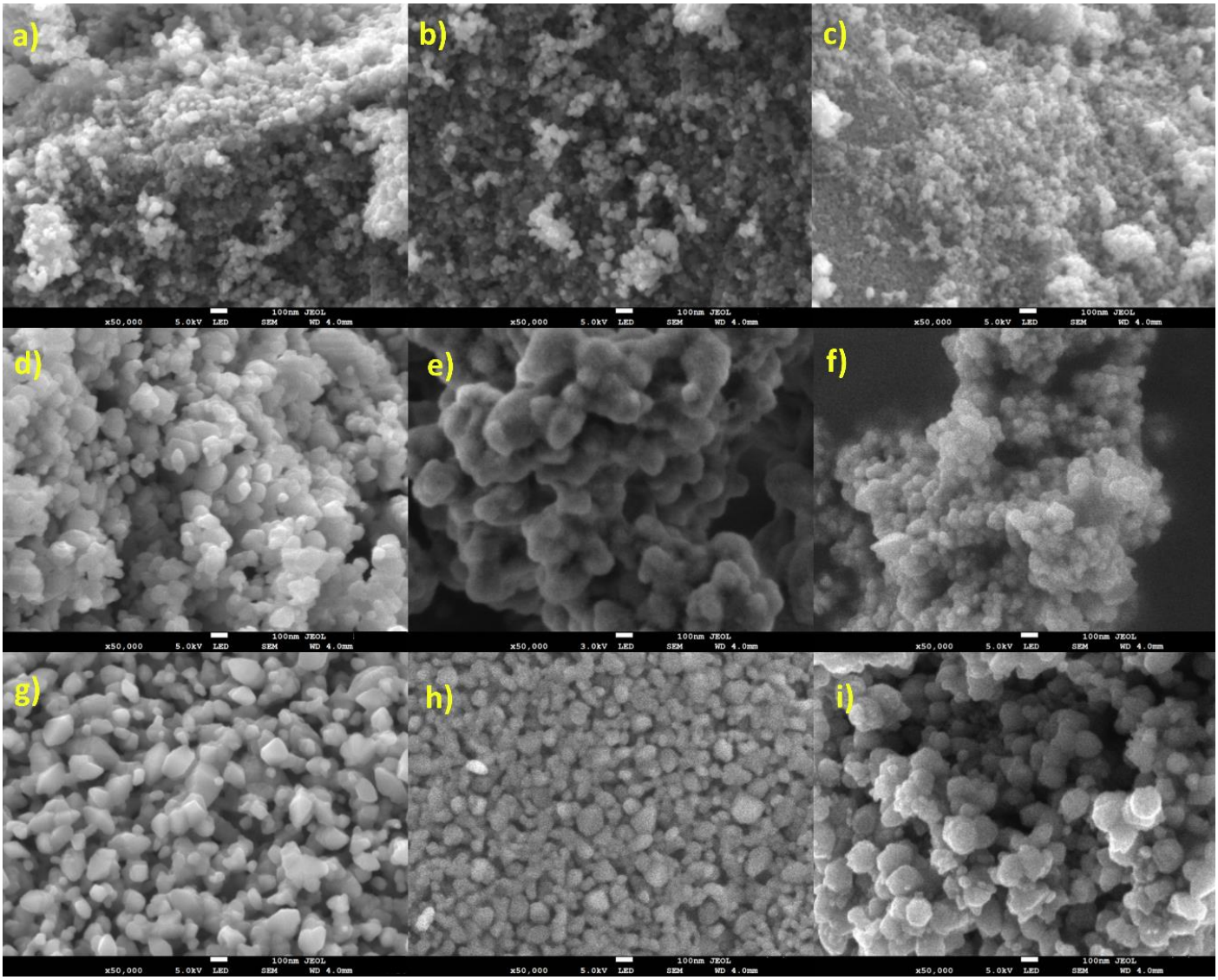

Figure 3 SEM images for TiO_2 and Srilankite samples. TiO_2 a)-c), ZrO_2-TiO_2_1-3 d)-f) and ZrO_2-TiO_2_1-4 g)-i).

Preprints (www.preprints.org) | NOT PEER-REVIEWED | Posted: 8 July 2020 doi:10.20944/preprints202007.0158.v1

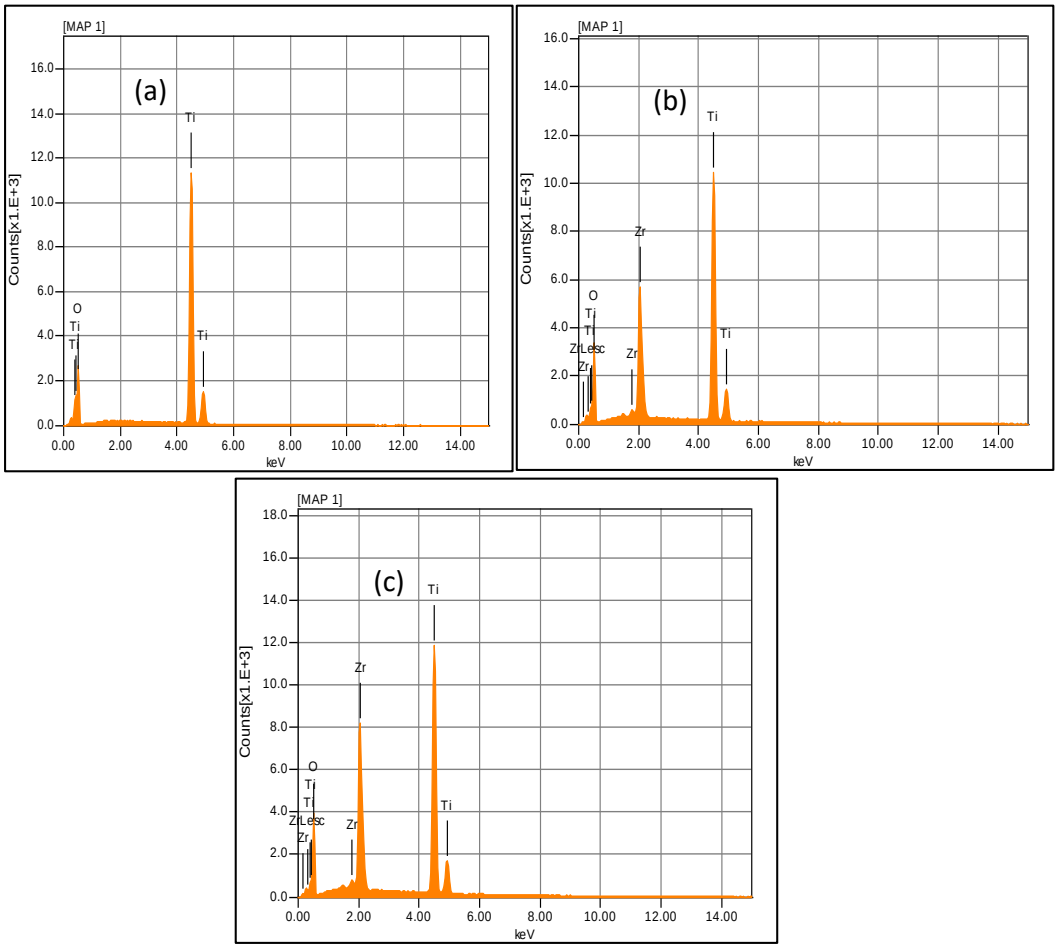

Figure 4 EDS spectra for a) TiO_2, b) ZrO_2/TiO_2_1-3 and c) ZrO_2/TiO_2_1-4.

Table 4. Normalized composition of the catalytic materials TiO_2, ZrO_2/TiO_2 1:3, and ZrO_2/TiO_2 1:4 obtained from EDS analysis.

Sample	*Element*	*Average Weight %*
TiO_2	O	42.03
	Ti	57.97
ZrO_2-TiO2 1:3	O	35.18
	Ti	38.51
	Zr	26.31
ZrO_2-TiO_2 1:4	O	36.51
	Ti	41.23
	Zr	22.25

3.2 Effect of the catalyst.

Figure 5 shows the performance of the catalysts labeled as a)TiO_2, b)TiO_2_1.5M, c)ZrO_2-TiO_2 1:3_1.5M, and d)ZrO_2-TiO_2 1:4_1.5M of the esterification reaction. The reaction was carried out using a 5 % weight of the catalyst concerning FFA. The plots show FFA percentage (95 % in all cases) vs. the reaction time ●(360 minutes in all cases) and the percentage conversion of FFA vs. the reaction time ■.

Preprints (www.preprints.org) | NOT PEER-REVIEWED | Posted: 8 July 2020 doi:10.20944/preprints202007.0158.v1

The final conversion of the catalysts corresponds to a)70. 5 %, b)88.8 %, c)86.8 %, and d)90.1 %. It is clear the lower conversion of the TiO_2 (70.5 % of conversion); however, this increases (at 88.8 %) after the sulfation. The reactions present a slightly lower for the sample ZrO_2-TiO_2 1:3 (Figure 5c), but, it is possible to observe in the short reaction times of 120 minutes that ZrO_2/TiO_2 1:4 reached a higher conversion, close to 75%, 10% higher than the other two materials.

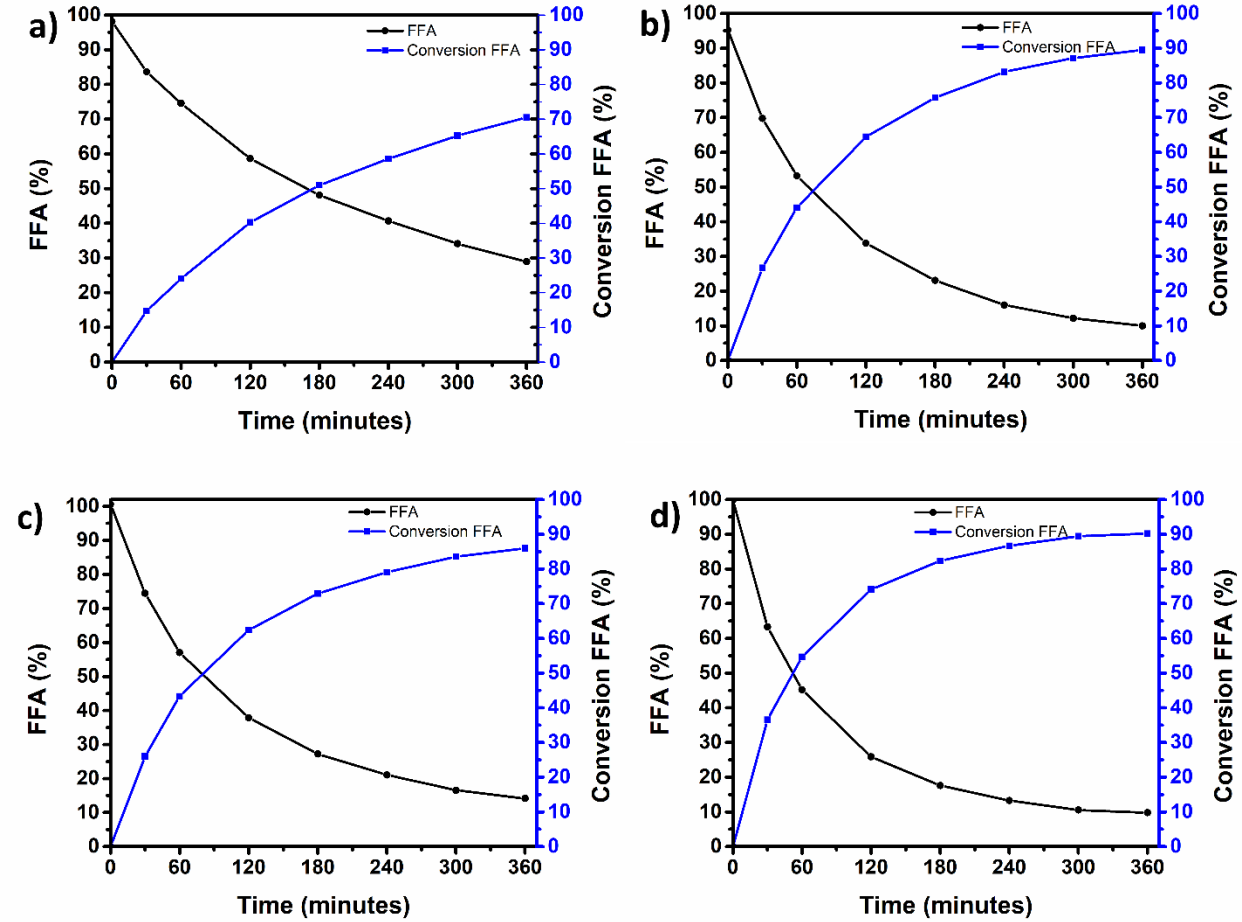

Figure 5 Efficiency of conversion of FFA for a)TiO2, b)TiO2_1.5M, c)ZrO2-TiO2 1:3_1.5M, and d)ZrO2-TiO2 1:4_1.5M of the esterification reaction

From above, it is possible to establish a high conversion efficiency in the phases Srilankite labeled as ZrO_2-TiO_2_1-4_1.5M and ZrO_2/TiO_2_1-3_1.5M, this may be related to the following reasons:

1) the increase of surface area due to the nano-crystalline structure of the catalyst and the acid sites (active sites), dispersed in large surface area, thus providing higher volume surface to facilitate the diffusion of reactants and reagent molecules[39].

2) The high number of sulfated ions increase the acid strength of the catalyst and has more significant catalytic activity. This effect maintains the same behavior as found by Li *et al.* (2012), where the conversion of lactic acid was directly proportional to a higher amount of the catalyst [25].

Furthermore, these results reflect a correlation similar to Carlucci *et al.* (2019) [40], where sulfate ions improve the surface acidity to the solid matrix. These ions are adhered to through structural bridges with the metal oxides, and, this coordination improves to specific molar ratios of Zr/Ti.

4. Conclusions

By the Sol-Gel method, TiO_2 and Srilankite nanoparticles were synthesized; the crystal structures corresponded to an admix of phases Anatase/rutile and admix of phase Silankite/rutile, respectively. After obtaining the catalysts, these where sulfated by a solution of H_2SO_4 at different

concentrations (0.5 M, 1.0 M, and 1.5 M), where the better results found to be at 1.5 M concentration. The sulfur ions within the TiO_2 and Srilankite sites were absorbed, which were verified by the FTIR analysis.

During the esterification reaction, the sample (Srilankite/rutile), with the biggest nanoparticles, showed good efficient catalytic activity (90% conversion). It is attributable to the high number of sulfur ions, which demonstrates the high potential of this catalyst (sample ZrO2-TiO2 1:4_1.5M); therefore, with this compound, it would be a good alternative in the reaction of esterification.

Supplementary Materials: The following are available online at www.mdpi.com/xxx/s1, Figure S1: title, Table S1: title, Video S1: title.

Author Contributions: Conceptualization, L.R.B. and S.J.S.F; Formal analysis, Y.S.R. and I.Z.T.; Funding acquisition, G.P.H.; Investigation, R.B.H.; Methodology, G.T.H.; Project administration, G.P.H.; Supervision, E.R.M.; Validation, Y.C.P.L; Writing – original draft, E.R.M.; Writing – review & editing, I.Z.T.

Funding: This research was funded by SEP-CONACyT, grant number 286165

Acknowledgments: The authors gratefully acknowledge the financial support from the Mexican Council for Science and Technology Moreover, the first author acknowledges CONACyT for his graduate fellowship.

Conflicts of Interest: The authors declare no conflict of interest.

References

1. Liu, F.; Ma, X.; Li, H.; Wang, Y.; Cui, P.; Guo, M.; Yaxin, H.; Lu, W.; Zhou, S.; Yu, M. Dilute sulfonic acid post functionalized metal organic framework as a heterogeneous acid catalyst for esterification to produce biodiesel. *Fuel* **2020**, *266*, 117149.
2. Zhang, Q.; Zhang, Y.; Deng, T.; Wei, F.; Jin, J.; Ma, P. *Sustainable production of biodiesel over heterogeneous acid catalysts*; Elsevier B.V., 2020; ISBN 9780444643070.
3. Rashid, U.; Soltani, S.; Al-Resayes, S.I.; Nehdi, I.A. Metal oxide catalysts for biodiesel production. In *Metal Oxides in Energy Technologies*; Wu, Y., Ed.; Elsevier: Amsterdam, Netherlands, 2018; pp. 303–319 ISBN 9780128111673.
4. Mongkolbovornkij, P.; Champreda, V.; Sutthisripok, W.; Laosiripojana, N. Esterification of industrial-grade palm fatty acid distillate over modified ZrO2 (with WO3–, SO4 –and TiO2–): Effects of co-solvent adding and water removal. *Fuel Process. Technol.* **2010**, *91*, 1510–1516.
5. Kaur, N.; Ali, A. Preparation and application of Ce/ZrO2-TiO2/SO42- as solid catalyst for the esterification of fatty acids. *Renew. Energy* **2015**, *81*, 421–431.
6. Shimada, G.B.; Cestari, A. Synthesis of heterogeneous catalysts by the hydrolytic Sol-Gel method for the biodiesel production. *Renew. Energy* **2020**, *156*, 389–394.
7. Thoai, D.N.; Tongurai, C.; Prasertsit, K.; Kumar, A. A novel two-step transesterification process catalyzed by homogeneous base catalyst in the first step and heterogeneous acid catalyst in the second step. *Fuel Process. Technol.* **2017**, *168*, 97–104.
8. Gu, L.; Huang, W.; Tang, S.; Tian, S.; Zhang, X. A novel deep eutectic solvent for biodiesel preparation using a homogeneous base catalyst. *Chem. Eng. J.* **2015**, *259*, 647–652.
9. Li, X.; Lan, X.; Wang, T. Selective oxidation of furfural in a bi-phasic system with homogeneous acid catalyst. *Catal. Today* **2016**, *276*, 97–104.
10. Mekala, M.; Goli, V.R. Kinetics of esterification of methanol and acetic acid with mineral homogeneous acid catalyst. *Chinese J. Chem. Eng.* **2015**, *23*, 100–105.
11. Rönnback, R.; Salmi, T.; Vuori, A.; Haario, H.; Lehtonen, J.; Sundqvist, A.; Tirronen, E. Development of a kinetic model for the esterification of acetic acid with methanol in the presence of a homogeneous acid catalyst. *Chem. Eng. Sci.* **1997**, *52*, 3369–3381.

12. de Almeida, R.M.; Noda, L.K.; Gonçalves, N.S.; Meneghetti, S.M.P.; Meneghetti, M.R. Transesterification reaction of vegetable oils, using superacid sulfated TiO2–base catalysts. *Appl. Catal. A Gen.* **2008**, *347*, 100–105.
13. Kazemian, H.; Turowec, B.; Siddiquee, M.N.; Rohani, S. Biodiesel production using cesium modified mesoporous ordered silica as heterogeneous base catalyst. *Fuel* **2013**, *103*, 719–724.
14. Nath, B.; Das, B.; Kalita, P.; Basumatary, S. Waste to value addition: Utilization of waste Brassica nigra plant derived novel green heterogeneous base catalyst for effective synthesis of biodiesel. *J. Clean. Prod.* **2019**, *239*, 118112.
15. Pradhan, S.; Sahu, V.; Mishra, B.G. CaO-ZrO2 nanocomposite oxide prepared by urea hydrolysis method as heterogeneous base catalyst for synthesis of chromene analogues. *J. Mol. Catal. A Chem.* **2016**, *425*, 297–309.
16. Shibasaki-Kitakawa, N.; Tsuji, T.; Kubo, M.; Yonemoto, T. Biodiesel Production from Waste Cooking Oil Using Anion-Exchange Resin as Both Catalyst and Adsorbent. *BioEnergy Res.* **2011**, *4*, 287–293.
17. Li, Y.; Zhang, X.-D.; Sun, L.; Zhang, J.; Xu, H.-P. Fatty acid methyl ester synthesis catalyzed by solid superacid catalyst /ZrO2–TiO2/La3+. *Appl. Energy* **2010**, *87*, 156–159.
18. Wong, W.Y.; Lim, S.; Pang, Y.L.; Shuit, S.H.; Chen, W.H.; Lee, K.T. Synthesis of renewable heterogeneous acid catalyst from oil palm empty fruit bunch for glycerol-free biodiesel production. *Sci. Total Environ.* **2020**, *727*, 138534.
19. Pandian, S.; Sakthi Saravanan, A.; Sivanandi, P.; Santra, M.; Booramurthy, V.K. *Application of heterogeneous acid catalyst derived from biomass for biodiesel process intensification: a comprehensive review*; Elsevier Inc., 2020; ISBN 9780128189962.
20. Gan, S.; Ng, H.K.; Chan, P.H.; Leong, F.L. Heterogeneous free fatty acids esterification in waste cooking oil using ion-exchange resins. *Fuel Process. Technol.* **2012**, *102*, 67–72.
21. Yadav, M.; Singh, V.; Sharma, Y.C. Methyl transesterification of waste cooking oil using a laboratory synthesized reusable heterogeneous base catalyst: Process optimization and homogeneity study of catalyst. *Energy Convers. Manag.* **2017**, *148*, 1438–1452.
22. Mardhiah, H.H.; Ong, H.C.; Masjuki, H.H.; Lim, S.; Lee, H.V. A review on latest developments and future prospects of heterogeneous catalyst in biodiesel production from non-edible oils. *Renew. Sustain. Energy Rev.* **2017**, *67*, 1225–1236.
23. Liu, L.; Wang, F.-Y.; Shao, G.-S.; Yuan, Z.-Y. A low-temperature autoclaving route to synthesize monolithic carbon materials with an ordered mesostructure. *Carbon N. Y.* **2010**, *48*, 2089–2099.
24. Li, K.-T.; Wang, C.-K.; Wang, I.; Wang, C.-M. Esterification of lactic acid over TiO2–ZrO2 catalysts. *Appl. Catal. A Gen.* **2011**, *392*, 180–183.
25. Li, Z.; Wnetrzak, R.; Kwapinski, W.; Leahy, J.J. Synthesis and Characterization of Sulfated TiO 2 Nanorods and ZrO 2 /TiO 2 Nanocomposites for the Esterification of Biobased Organic Acid. *ACS Appl. Mater. Interfaces* **2012**, *4*, 4499–4505.
26. Ropero-Vega, J.L.; Aldana-Pérez, A.; Gómez, R.; Niño-Gómez, M.E. Sulfated titania [TiO2/SO42−]: A very active solid acid catalyst for the esterification of free fatty acids with ethanol. *Appl. Catal. A Gen.* **2010**, *379*, 24–29.
27. Xie, W.; Zhao, L. Heterogeneous CaO–MoO3–SBA-15 catalysts for biodiesel production from soybean oil. *Energy Convers. Manag.* **2014**, *79*, 34–42.
28. Singh, L.P.; Bhattacharyya, S.K.; Kumar, R.; Mishra, G.; Sharma, U.; Singh, G.; Ahalawat, S. Sol-Gel processing of silica nanoparticles and their applications. *Adv. Colloid Interface Sci.* **2014**, *214*, 17–37.

29. Lónyi, F.; Valyon, J. Thermally effected structural and surface transformations of sulfated TiO2, ZrO2 and TiO2-ZrO2 catalysts. *J. Therm. Anal.* **1996**, *46*, 211–218.
30. Pérez-Jiménez, L.E.; Solis-Cortazar, J.C.; Rojas-Blanco, L.; Perez-Hernandez, G.; Martinez, O.S.; Palomera, R.C.; Paraguay-Delgado, F.; Zamudio-Torres, I.; Morales, E.R. Enhancement of optoelectronic properties of TiO2 films containing Pt nanoparticles. *Results Phys.* **2019**, *12*, 1680–1685.
31. Davar, F.; Hassankhani, A.; Loghman-Estarki, M.R. Controllable synthesis of metastable tetragonal zirconia nanocrystals using citric acid assisted sol–gel method. *Ceram. Int.* **2013**, *39*, 2933–2941.
32. Praveen, P.; Viruthagiri, G.; Mugundan, S.; Shanmugam, N. Structural, optical and morphological analyses of pristine titanium di-oxide nanoparticles – Synthesized via sol–gel route. *Spectrochim. Acta Part A Mol. Biomol. Spectrosc.* **2014**, *117*, 622–629.
33. Alamgir; Khan, W.; Ahmad, S.; Mehedi Hassan, M.; Naqvi, A.H. Structural phase analysis, band gap tuning and fluorescence properties of Co doped TiO2 nanoparticles. *Opt. Mater. (Amst).* **2014**, *38*, 278–285.
34. Shi, W. Zr-La doped sulfated titania with a by far better catalytic activity and stability than pure sulfated titania in the esterification of acetic acid and n-butanol. *Catal. Letters* **2013**, *143*, 732–738.
35. Al-Asbahi, B.A. Influence of anatase titania nanoparticles content on optical and structural properties of amorphous silica. *Mater. Res. Bull.* **2017**, *89*, 286–291.
36. Hojamberdiev, M.; Zhu, G.; Sujaridworakun, P.; Jinawath, S.; Liu, P.; Zhou, J.-P. Visible-light-driven N–F-codoped TiO2 powders derived from different ammonium oxofluorotitanate precursors. *Powder Technol.* **2012**, *218*, 140–148.
37. Shao, G.N.; Imran, S.M.; Jeon, S.J.; Engole, M.; Abbas, N.; Salman Haider, M.; Kang, S.J.; Kim, H.T. Sol–gel synthesis of photoactive zirconia–titania from metal salts and investigation of their photocatalytic properties in the photodegradation of methylene blue. *Powder Technol.* **2014**, *258*, 99–109.
38. Saravanan, K.; Tyagi, B.; Bajaj, H.C. Nano-crystalline, mesoporous aerogel sulfated zirconia as an efficient catalyst for esterification of stearic acid with methanol. *Appl. Catal. B Environ.* **2016**, *192*, 161–170.
39. Carlucci, C.; Degennaro, L.; Luisi, R. Titanium dioxide as a catalyst in biodiesel production. *Catalysts* **2019**, *9*.
40. Das, D. Preparation, physico-chemical characterization and catalytic activity of sulphated ZrO2–TiO2 mixed oxides. *J. Mol. Catal. A Chem.* **2002**, *189*, 271–282.